Piezoelectricity and ferroelectricity in biomaterials: Molecular modeling and piezoresponse force microscopy measurements

V. S. Bystrov' , E. Seyedhosseini, S. Kopyl, I. K. Bdikin, and A. L. Kholkin

Citation: Journal of Applied Physics **116**, 066803 (2014); doi: 10.1063/1.4891443
View online: http://dx.doi.org/10.1063/1.4891443
View Table of Contents: http://aip.scitation.org/toc/jap/116/6
Published by the American Institute of Physics

JOURNAL OF APPLIED PHYSICS **116**, 066803 (2014)

Piezoelectricity and ferroelectricity in biomaterials: Molecular modeling and piezoresponse force microscopy measurements

V. S. Bystrov,[1,2,a)] E. Seyedhosseini,[1] S. Kopyl,[3] I. K. Bdikin,[3] and A. L. Kholkin[1]
[1]*Department of Materials Engineering and Ceramics & CICECO, University of Aveiro, 3810 193 Aveiro, Portugal*
[2]*Institute of Mathematical Problems of Biology, Russian Academy of Sciences, 142290 Pushchino, Moscow region, Russia*
[3]*TEMA NRD, Mechanical Engineering Department, Aveiro Institute of Nanotechnology (AIN), University of Aveiro, 3810 193 Aveiro, Portugal*

(Received 12 February 2014; accepted 15 July 2014; published online 11 August 2014)

Piezoelectricity is one of the important functional properties inherent to many biomaterials. It stems from the non-centrosymmetric crystal structure of most biopolymers including proteins, polysaccharides, and lipids. Understanding the relationship between the generated electric field and applied mechanical stress has become the main motivation to studying piezoelectricity in biological systems and artificial biomaterials at the nanoscale. In this work, we present a review of the piezoelectric and ferroelectric properties of several molecular systems and nanomaterials revealed by Piezoresponse Force Microscopy (PFM) and compare the results with molecular modeling and computer simulations. Experimentally observed by PFM and calculated dielectric, piezoelectric, and ferroelectric properties of these materials are analyzed in the context of their possible role in functionality of biological systems. © *2014 AIP Publishing LLC*.
[http://dx.doi.org/10.1063/1.4891443]

I. INTRODUCTION

Creating artificial biomimetic materials with multiple functions similar to those of living bodies is an important frontier for advanced society in near future. Electromechanical coupling is one of the important properties of many organic and bioorganic materials[1,2] and is one of the essential features of biological and living systems, in particular, regarding their electrical and mechanical signalization.[3,4] It is based on the complex dipolar properties and dipole-dipole interactions conjugated with hydrogen bonds network in biomolecular systems with different levels of self-assembly and hierarchy. It has been recently shown[5,6] that several biomolecular structures (both crystalline and composite) based on important biological molecules demonstrate properties similar to their inorganic counterparts, namely, sufficiently strong piezoelectricity and, moreover, apparent ferroelectric-like behavior. We will start from the definition of piezoelectricity and ferroelectricity in general and historical overview of these phenomena observed in biological materials.

In a classical definition,[7] piezoelectricity is a linear coupling between mechanical stress and electric polarization (the direct piezoelectric effect) or between mechanical strain and applied electric field. It arises in crystalline materials with non-centrosymmetric structure due to asymmetric positions of atoms and ions. Direct and converse effects are described by the same coefficients.[8] This definition can still be applied to non-crystalline and complex composite materials of biological origin but only a phenomenological description is available because of the complexity of the phenomenon. Direct and converse effects are different and strongly depend on the measurement conditions and presence of water. Piezoelectricity in biological objects was first observed and described by Fukada in the 1950s, initially in wood,[9,10] and later in bone tissue.[11,12] Further, piezoelectricity and pyroelectricity were found in a number of biological materials of different nature.[13–21] Lang *et al.*[18] were the first to report piezoelectricity in calcification of the human pineal gland, demonstrating also non-centrosymmetric structure of the material by second harmonic generation (SHG) measurements. Recent measurements of piezoelectric effects in seashells[22] and human nails[23] confirmed ubiquitous presence of this coupling in bioobjects.

Even more exciting is the presence of a polar order in some biomaterials and their ability to switch their polarization under sufficiently high electric field. Again, in crystalline materials ferroelectricity suggests the presence of a long-range order in the regular positions of atoms and the symmetry loss at some critical temperature called Curie temperature.[7] The stability of ferroelectric phase thus decreases with temperature with a concomitant possibility of polarization reversal when the electric field exceeds some critical value called coercive field. In bioobjects, it is not necessarily the case and, typically, only the observation of the polarization (or piezocoefficient) hysteresis serves as a proof of a ferroelectric behavior. In fact, presence of ferroic activity, including elastic, electrical, and magnetic, has been strongly indicated in multitudes of floras and faunas around us[24] and is thought to be a universal property of all living organisms.[20] Recent discoveries of ferroelectric-like behavior in aortic walls[25] and elastin[26] provoked a new wave of interest to these phenomena, generally called *bioferroelectric* in the literature. Further generalization of the term bioferroelectricity can be found, for

[a)]bystrov@ua.pt

example, in voltage-controlled muscle movement, in the excitable biological membranes[27] and in the voltage-dependent ion channels.[5,13] Brain memory was thought to be based on a ferroelectric mechanism.[28] In the series of articles by Beresnev *et al.*,[29] close similarity between biomembranes and ferroelectric liquid crystals (tilted layers of lipid and protein molecules alignment) was noted. Leuchtag[13] was the first who considered dielectric constant ε as a nonlinear function of electric field in the classical electrodiffusion model to explain the membrane function. He analyzed and fitted the existing ion-channel data[30] with the Curie-Weiss law (apparent manifestation of ferroelectricity) in biomembranes. Ermolina *et al.*[31] observed a liquid-crystal-like ferroelectric behavior in bacteriorhodopsin, an integral protein of the purple membrane of *Halobacterium salinarium*, embedded into the lipid biomembrane. Similarly, the Curie-Weiss law was valid suggesting apparent ferroelectric-like behavior.[32] According to Brown and Tuszynski,[33,34] ferroelectricity and piezoelectricity accounts for the coupling of dipolar tubulin molecular dimers to conformational states in microtubules intracellular skeleton and protein moving system in each living cell. All these phenomena are essential for many complex bioobjects but cannot be strictly called ferroelectric in a classical sense because of the variety of different mechanisms involved (due to, e.g., flexoelectricity in membranes or presence of water in bone). This makes the assignment of biological phenomena under electric field to ferroelectricity difficult, and sometimes speculative. The hindrance in ferroelectric hypothesis was also due to the fact that biological samples being soft could not endure the mechanical force required for electromechanical measurement and are subject to strong electrostatic effect (Maxwell force). Another obstacle was the inability to look at the nanoscale to assign the observed complex electromechanical behavior to the particular structure unit and thus to understand the mechanism of the polar behavior and polarization reversal.

The studies of the piezoelectric and ferroelectric properties of biomaterials at the nanoscale have become possible only recently thanks to the fast developments of Scanning Probe Microscopy including Piezoresponse Force Microscopy (PFM) and Switching Spectroscopy PFM.[35,36] From the very beginning, these techniques were widely applied for the study of biological objects.[37,38] Only using PFM techniques, it was possible to obtain piezoelectric hysteresis loops (that are supposed to be a signature of ferroelectricity) in aorta walls[25] and elastin[26] of mammals. In a review of this finding, Chen and Gao[39] noted that ferroelectricity function could serve as a critical component in a local integrated memory-like structure, together with nerves in the aorta. This interesting observation has led us to believe that the constituents of proteins such as amino acids, lipids, and amyloid-like structures could be responsible for ferroelectricity and, as such, should be studied first to understand the global behavior of the complex biological systems. This review is thus devoted to recent findings of the piezoelectric and ferroelectric features in artificial structures based on crystalline amino acids (glycine),[40] peptides (self-assembled nanotubes),[41] and lipid/ferroelectric bilayers.[42] We hope that the understanding of the electromechanical behavior in these structures under an applied electric field will open a pathway for further insight to piezoelectric and ferroelectric phenomena in complex biological materials.

II. LIPIDS NANO-STRUCTURES: FERROELECTRIC ORDERING AND PROPERTIES

Lipids are the main constituents of biological cell membranes, and their liquid crystalline properties play a crucial role in cell functions. Most of them have dipole moments[43] and thus could have polar properties, which offer a possibility for piezoelectric and ferroelectric behaviors that can be revealed by PFM. Lipids usually form liquid crystal structures.[44] Liquid crystals represent a unique segment of soft matter. Various organic molecules with different shapes, such as rods, disks, or bent-core (pyramid or banana-shaped) molecules[45,46] form a large number of liquid crystalline mesophases with properties determined by the temperature. In such thermotropic liquid crystals, the orientational order is dictated by the shape of the molecules and the mobility is given by the thermal motion. Recent observations[47] indicate that glycolipid molecules self-assemble into the pairs of tilted and antiferroelectric double layers sandwiched between layers of bent-core molecules. These systems provide a basis for the understanding of bioferroelectricity, which may be important for biological cell membrane functions.

A. Liquid crystalline and ferroelectric properties of lipids

As was pointed out earlier,[47] the dodecyl-b-D-glucopyranoside glycolipid layers can be electrically polarized in supramolecular structures of glycolipid and bent-core ("banana-shape") molecules, forming ferroelectric/antiferroelectric structures. Considering lipids structures, we must note that glycolipid molecules contain polar (hydrophilic) sugar head groups and antipolar (hydrophobic) carbon chains, i.e., they are amphiphilic. They form liquid crystalline structures in aqueous systems depending on the concentration, as well as in their pure state depending on temperature, i.e., they are also amphotropic liquid crystals.[44] Lyotropic liquid crystals appear in the nature in living organisms.[46] Liquid crystalline properties of lyotropic synthetic glycolipids have been rigorously studied in Ref. 47. Glycolipid[43] is one of the three lipids that makes up the biological cell membranes. Other important lipids in cell membranes are phospholipids and steroids.[43] The complex glycolipids (starting with three sugar head groups) are involved in cell surface recognition processes.[48] Most of these processes are electrical, for example, ferroelectric-like behavior was seen in nerves and muscle membranes.[13,14] Some reports[47] described how the glycolipid molecules (specifically alkyl glucoside, the simplest class of glycolipids with one sugar polar headgroup and an apolar carbon chain) aggregate into antiferroelectric supramolecular structures in correlation with bent-core molecules. Smectic liquid crystals of bent-core ("banana-shape") molecules recently attracted considerable interest because of their ferroelectric properties[49] due to the formation of chiral superstructures.[50]

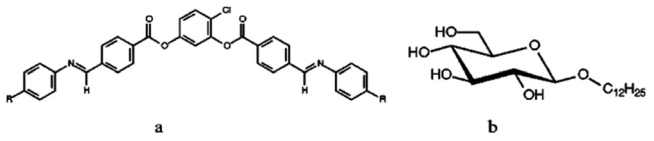

FIG. 1. The molecular structures of the components of the studied mixtures: (a) Molecular structure of the bent shape liquid crystalline compound (*R* C14H29): 4 chloro phenyline bis [4 (4 n tetradecyloxypheylimino methyl) benzoate] (BO14Cl). (b) Molecular structure of dodecyl b D gluco pyranoside (C12G1). Reproduced by permission from Abeygunaratne *et al.*, Phys. Rev. E **69**, 021703 (2004). Copyright 2004 by IOP Publishing.

B. Antiferroelectric ordering of amphiphilic glycolipids in bent-core liquid crystals

Binary mixtures of bent-core liquid crystalline molecules 4-chloro-phenyline-bis [4 (4-n-tetradecyloxypheylimi-nomethyl)-benzoate][47,51] (hereafter we will refer to it as BO14Cl), and dodecyl b-−D-glucopyranoside (referred as C12G1), which has a glucose polar hydrophilic head group and a hydrophobic alkyl chain with 12 carbon atoms (Fig. 1), were extensively studied for various concentrations. The time dependence of the electric current under triangular voltage excitations reveals an antiferroelectric-type polarization switching of mixtures with less than 70 wt. % C12G1 concentrations (Fig. 2(a)). The temperature dependences of the polarization, as determined from the area under the polarization current peaks, are shown in Fig. 2(b). The most interesting result obtained in Ref. 47 is that the macroscopic polarization of the bent-core liquid crystalline material is unaffected even when it is diluted up to 60 wt. % of the lipid molecules. The C12G1 molecules themselves form macroscopically non-polar structure, where the polar sugar heads facing in opposite directions (opening angle $\theta = 180°$) in non-tilted double layer configuration. It is apparent that in the bent-core BO14Cl environment, the lipid double layers adopt the tilted configuration with the polar heads tilted with respect to each other. This indicates that the polar sugar heads of the C12G1 molecules become tilted with respect to each other (opening angle: $\theta < 180°$). To estimate this angle, Abeygunaratne *et al.*[47] calculated the molecular dipoles of the C12G1 molecules as $\mu P = 3.25$ $D = 1.08 \times 10^{29}$ Cm. Taking into account that the molecular weight of C12G1 is 348, and the mass density is about 1 g/cm^3, they show that uniformly arranged dipoles would result in polarization value $P_o = 2 \times 10^{2}$ C/m^2 $= 2 \times 10^3$ nC/cm^2. The effective polarization of the bent double layer configuration can be given as $Pk = Po \cdot \cos(b/2)$ (k stands for a kink). The observation that the contribution of the bent lipid double layers to

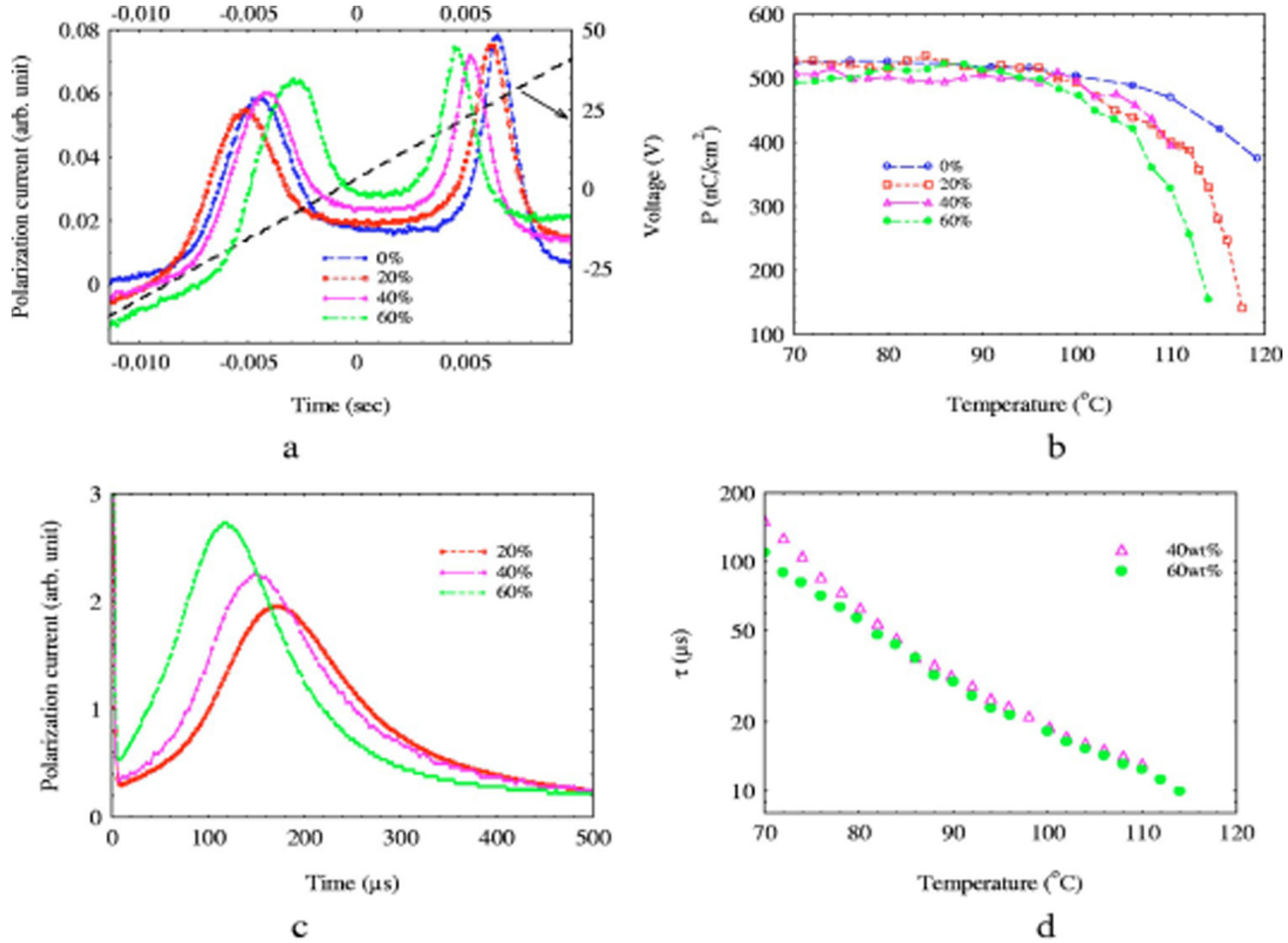

FIG. 2. (a) Polarization current curves at 70 °C of the mixtures with different concentrations under triangular fields of 10 V/cm amplitude. (b) Temperature de pendence of the polarization for different concentrations of C12G1. (c) Time dependences of the polarization current for different concentrations after fast electric field reversal E 10 V/cm. (d) Temperature dependence of the switching time for two different concentrations. Reproduced by permission from Abeygunaratne *et al.*, Phys. Rev. E **69**, 021703 (2004). Copyright 2004 by IOP Publishing.

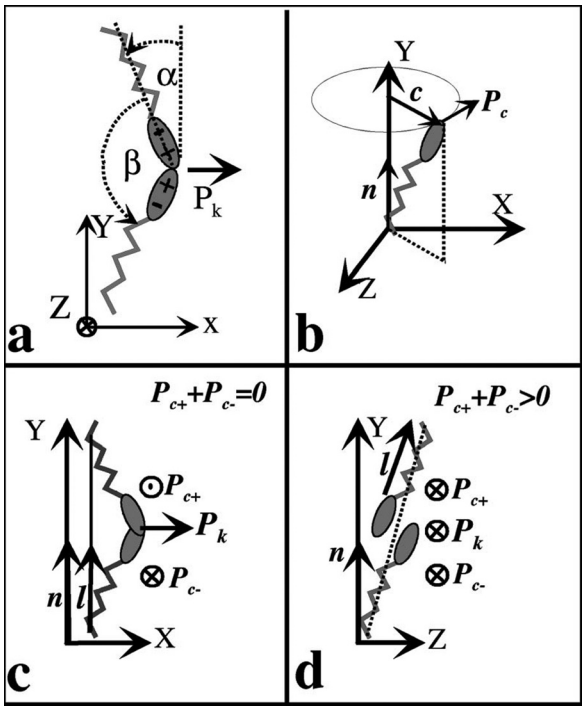

FIG. 3. Proposed model for the packing of the C12G1 molecules. The dodecyl b D glucopyranoside molecules form bent smectic double layers mimicking the structure of the bent and tilted banana shape molecules. The darker areas indicate parts tilted away the observer viewing the material along the smectic layers. P_k is the polarization of the glycolipids due to the kinked polar heads. (b) Polarization $P_c \infty cXn$ of tilted glycolipid layers due to molecular chirality and director tilt. (c) The direction of P_k and $P_c + (P_c\ )$ of the upper (lower) chiral lipid molecules in the SmA*P* configu ration; the direction of P_k and $P_c + (P_c\ )$ of the upper (lower) chiral lipid molecules in the Sm*CP* configuration. Reproduced by permission from Abeygunaratne *et al*., Phys. Rev. E **69**, 021703 (2004). Copyright 2004 by IOP Publishing.

the polarization is basically equal to that from banana-shape molecules, i.e., $Pb \sim Pk = 500$ nC/cm^2 (b stands for banana) provides that the opening angle $\theta \sim 150°$ (Fig. 3(a)).

Abeygunaratne *et al*.[47] also proposed that the glycolipid molecules form the individual smectic double layers in between the layers of the banana-shaped molecules (Fig. 4). In this "interlayer" packing, the width of the C12G1 layers do not have to be a half of the BO14Cl layers, and the flexible alkyl chains of both kinds of molecules meet only other alkyl chains, which is a much more favorable packing. We note that it is necessary to form pairs of glycolipid double layers to ensure the experimentally observed antiferroelectric ground state. Such packing means layered nanostructures where the distance between the layers of the same type is determined by the concentration. Taking into account that the molecular weight of C12G1 is 348 and of BO14Cl is 950, in the highest "banana" dominating (~60-wt. % C12G1) concentration there is only one BO14Cl layer in between stacks of four C12G1 layers (Fig. 4). For lower glycolipid concentrations, each C12G1 stacks are separated by one or more BO14Cl layers. The observation that the periodicity of 34.2 Å is equal to that of the pure lipid, but smaller than the length of two fully stretched C12G1 molecules (38.4 Å), may indicate uncorrelated tilted (de Vries-type) smectic A phase. In this context, it is desirable to study structures in the lipid-dominated regime and in other "biofriendly" banana liquid crystals (for example without chlorine atoms) and various glycolipid derivatives. It would also be interesting to investigate whether the straight-core molecules are able to impose their order into amphiphilic systems. The expected ferroelectric properties in such layers could help to understand the functioning of actual lipid biological membrane in a living cell. Usually, this biological membrane of cells consists of the mixtures of several types

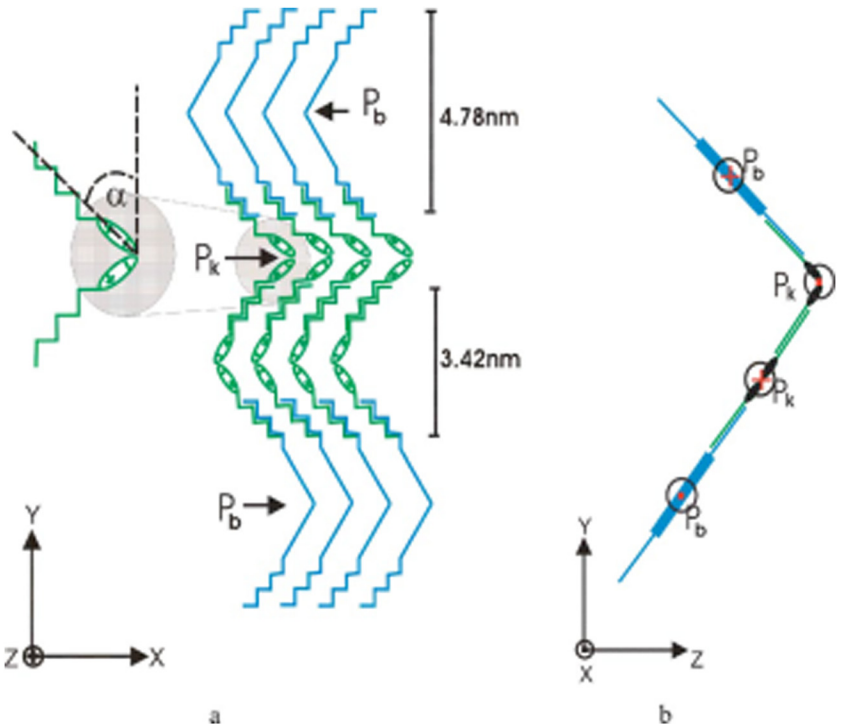

FIG. 4. Proposed model for the pack ing of the C12G1 molecules together with the BO14Cl molecules in the highest concentration (60 wt. %C12G1140 wt. %BO14Cl), where the bent core molecules still dominate the phase structure. P_b is the polariza tion due to the polar packing of banana shaped molecule. (a) Structure viewing normal to the kink and the bend polarization. (b) Structure view ing along the electric polarizations. Reproduced by permission from Abeygunaratne *et al*., Phys. Rev. E **69**, 021703 (2004). Copyright 2004 by IOP Publishing.

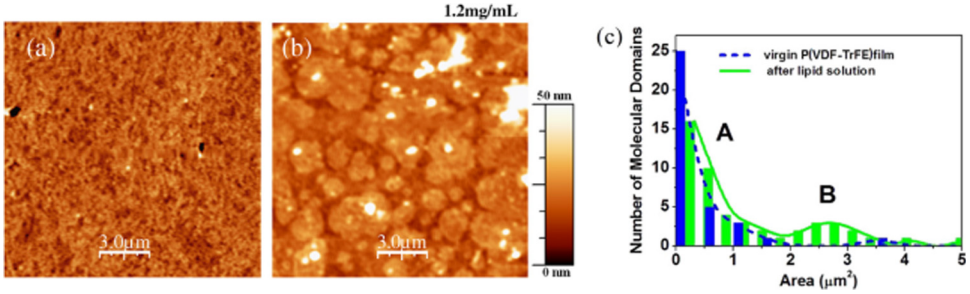

FIG. 5. (a) Topography of bare P(VDF TrFE) film, self assembled phospholipids on P(VDF TrFE) surface (b) and grain size distribution (c) of bare P(VDF TrFE) (A) and of self assembled phospholipid molecular domains (B) on P(VDF TrFE). Reproduced by permission from Heredia *et al.*, J. Phys. D **43**, 335301 (2010). Copyright 2010 by IOP Publishing.

of lipids and various functional proteins big molecular complexes, embedded into lipids bi-layers.

C. Deposition of phospholipids onto ferroelectric P(VDF-TrFE) films

One of the interesting and effective approaches to study polarization and piezoelectric properties of the molecular structures is to combine it with other ferroelectrics having already known properties. It is also important that ferroelectric polarization can be used to assemble various organic and inorganic species and to create nanostructures with controlled properties (so-called polarization lithography). Following this approach, Heredia *et al.*[42] used poly(vinylidene fluoride-co-trifluoroethylene) P(VDF-TrFE), ultrathin films deposited by the Langmuir Blodgett (LB) technique. The nanoscale properties of P(VDF-TrFE) LB layers were reported earlier.[52,53] These layers were used as templates for the assembly of various phospholipids, which are essential components of living cell membranes. It was observed that 1,2-di-*O*-hexadecyl-*sn*-glycero-3-phosphocholine phospholipids (DHPC) form self-assembled structures (molecular domains) on bare P(VDF-TrFE) surfaces. These were revealed by the formation of homogeneous and stable rounded blobs with diameters in the range 0.2 3 μm. Figures 5(a) and 5(b) show a change in the topography image when very smooth P(VDF-TrFE) template film is covered with the phospholipids. Self-assembly is noticeable after the phospholipid deposition at the concentration of 1.2 mg/ml. The size distribution of the molecular domains reveals additional maximum B (Fig. 5(c)) due to self-assembly; however, blobs with smaller diameters are abundant on the surface. The assembly of DHPC is apparently driven by intermolecular bonding, although a weak interaction with the P(VDF-TrFE) substrate is decisive for the nucleation of the observed domains. The formation process of lipid domains is currently unclear, although it might be possible that the polarization domains and associated stray electric fields from the P(VDF-TrFE) could significantly affect the assembly of phospholipids via electrostatic interaction.[54]

In another experiment, ferroelectric polymer films were polarized by the application of various voltages via a conducting tip using a home-made PFM setup and PFM images were then obtained showing controlled polarization distribution. After this, phospholipid molecules were deposited from the solution. Conventional AFM experiments were performed to assess the selectivity of the deposition process. It was observed that the deposition process is very sensitive to the concentration of the solution. It was established that the thickness of the deposited layers at high concentration was too big, so that it masked the selective deposition due to polarization patterning. The maximum effect was observed for the solution with the concentration of 1.5 mg/ml where the apparent stripes of the deposited materials are clearly seen on the topography image (Fig. 6(c)). The selective deposition was observed mainly at the polarization boundaries where the selectivity reached a maximum value of about 20% 40%.

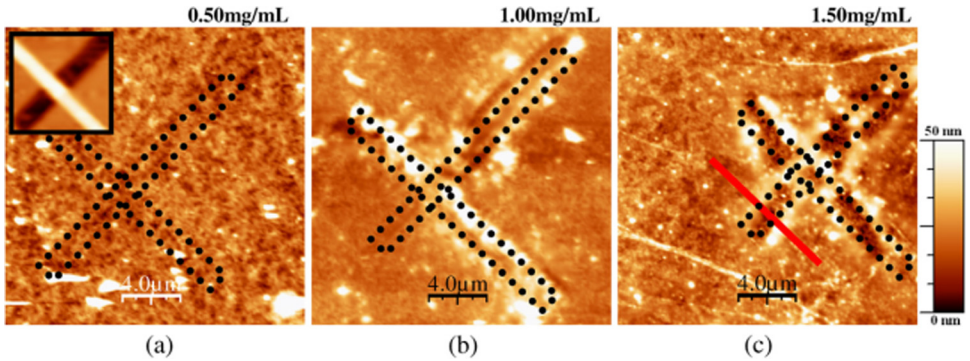

FIG. 6. Topography images of P(VDF TrFE) surface after the application of the phospholipidic solution of different concentrations (a), (b), (c) for 10 s (concentrations of the solutions are labelled on the images). Inset to (*a*) shows initial polarization patterns on P(VDF TrFE) written with +50 V and 50 V. Red solid line in (c) denotes PFM signal cross section shown in Figure 7(a). Reproduced by permission from Heredia *et al.*, J. Phys. D **43**, 335301 (2010). Copyright 2010 by IOP Publishing.

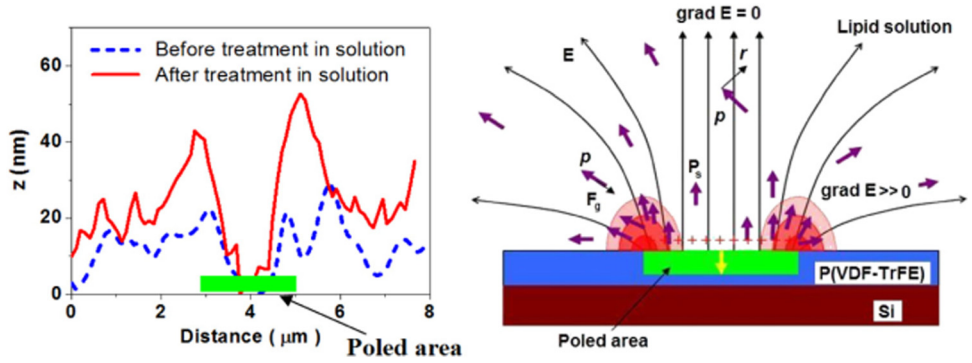

FIG. 7. (a) Topography cross section along the poled area before (dotted line) and after (solid line) the application of the phospholipid solution. (b) Schematic of the electric field distribution inside the lipid solution due to the poled P(VDF TrFE) area. Reproduced by permission from Heredia *et al.*, J. Phys. D **43**, 335301 (2010). Copyright 2010 by IOP Publishing.

These results suggest that the assembly is driven by the polarization boundaries, as the maximum height of the deposited phospholipids corresponds to the polarization domain edge (Fig. 7(a)). It thus can be stated that the polarization-driven assembly is governed by the polarization interfaces, suggesting that it is not the stray electric field itself, but its *gradient* that is responsible for selective deposition. The molecules are attracted by polarization lines (shown in the inset to Fig. 6(a)) as −PO3−4 polar heads or −NH+3 groups, and might feel the gradients of the stray field as is schematically shown in Fig. 7(b). Phospholipids possess a dipole moment (characterized by the value p) due to the charge distribution in the polar head. The attraction of the dipoles existing in the lipid solution due to the polarization of the P(VDF-TrFE) surface seems to be based on dielectrophoresis (DEP). In this case,[42] these dipole moments do already exist, thus increasing the potential of DEP for scaling down and using it for the manipulation of nanosized objects such as DNA, proteins, nanotubes, nanoparticles and, potentially, with small individual molecules in a solution. When placed in electric field E, equal but opposite forces arise on each side of the dipole creating a torque $\tau = p \times \mathrm{E}$. In a homogeneous electric field (grad$E = 0$), the dipole molecules do not move, because the total force acting on the molecule is zero ($Fg \sim p$ grad E). Apparently, the maximum gradient of electrical field and Fg exists near the polarization boundaries and thus can explain the observed effect (Fig. 7(b)). The results can be interpreted as follows: local poling of the P(VDF-TrFE) surfaces creates polarized areas that are associated with both polarization and screening charges that partly compensate each other. To evaluate the switching process of both bare P(VDFTrFE) films and those covered with phospholipid layers, piezoresponse hysteresis loops were acquired[35] when the PFM tip was stopped near a selected location and the voltage pulses of both polarities were sequentially applied between the tip and the bottom electrode (Fig. 8). The analysis of the hysteresis loops allows one to evaluate the dipole moment of the deposited phospholipid layer by the vertical offset of the loops based on the full switching polarization in P(VDF-TrFE).[52] As the relative piezoelectric offset (defined as Δd33/d33, see Fig. 8) is about 0.35, it translates to a polarization offset (i.e., the value of non-switchable part of polarization of the composite film) of about 3 μC/cm^2. This polarization is apparently due to the fixed (aligned) dipole moment of the phospholipid layer attached to the P(VDF-TrFE) surface. Further, we can roughly estimate the polarization value in phospholipids, using a molecular volume of 2 nm^3 and PO3−4 to NH+3 distance of about 0.5 nm, which gives the corresponding dipole moment of about 24 Debye. This results in the polarization of ≈4 μC/cm^2, quite close to experimental and calculated values.[53]

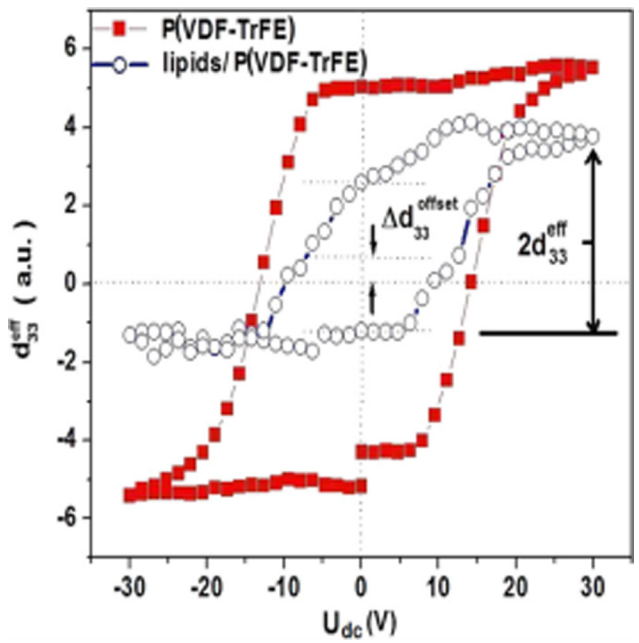

FIG. 8. Hysteresis curves of the local piezoresponse coefficient $(d_{33})_{\mathrm{eff}}$ measured as a function of the bias voltage U_{dc} in bare P(VDF TrFE) film and in phospholipid/P(VDF TrFE) composite. Vertical offset of $(d_{33})_{\mathrm{eff}}$ hys teresis is a measure of the non switchable polarization due to the presence of lipid layer. Reproduced by permission from Heredia *et al.*, J. Phys. D **43**, 335301 (2010). Copyright 2010 by IOP Publishing.

Further, the PFM experiments[42] were done by functionalized tip dipped into the DHPC solution and scanned on the P(VDFTrFE) surface to produce a patterned phospholipid region (white dotted line, Fig. 9(a)). The resulting black contrast in Fig. 9(b) signifies the polarization head terminated at the lipid layer. The black polarization lines (polarization with +50 V) can be seen *through* the lipid layer (Fig. 9(b)).

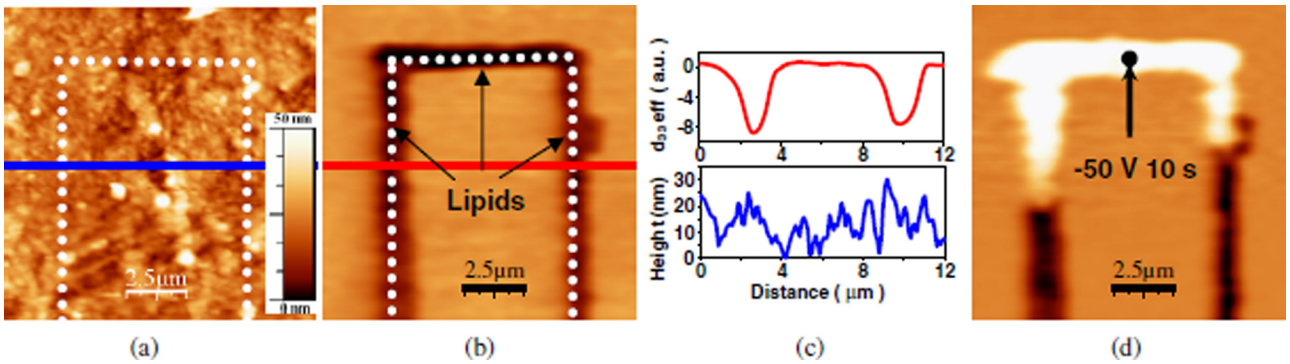

FIG. 9. Topography (a) and PFM image (b) of the preferred deposition of phospholipids on P(VDF TrFE) surface. Dotted line illustrates local deposition of lipids by the tip. (c) Cross sections of the PFM signal (top) and topography (bottom) images of (a) and (b). (d) PFM image after poling of the patterned lipid lines (white area). Reproduced by permission from Heredia *et al.*, J. Phys. D **43**, 335301 (2010). Copyright 2010 by IOP Publishing.

Then, the PFM tip was placed on the location marked with the black point (Fig. 9(d)) and −50 V was applied for 10 s. It is clearly seen that the switching occurs only in the areas covered by phospholipids following the polarization lines written in the previous experiment (white lines shown in Fig. 9(d)). No change in the polarization was observed beyond this line. This once again confirms preferred deposition of the lipids (though not seen on the topography, Fig. 6(c)) along the polarization lines, allowing the formation of complicated domain patterns. Easier switching of polarization in P(VDF-TrFE) in conjunction with the phospholipids is thus observed and might be useful for the study of the dynamics of ferroelectric domains in organic materials. PFM method is proved to be a very promising technique for untangling the electromechanical behavior in lipid-ferroelectric layers.

III. PIEZOELECTRICITY AND FERROELECTRICITY IN CRYSTALLINE GLYCINE

Many natural and artificial biomaterials consist of smaller building blocks, for example, amino acids.[5,6,15,43] All amino acids contains their own dipole moment (usually directed from oxygen to nitrogen atoms in its molecular structure), which leads to the complex dipole-dipole interactions and dipole ordering during self-assembly and formation of larger biomolecular systems. Recently, Lemanov *et al.*[55] have shown that several amino acids possess piezoelectric properties in the crystal form. Among them, the most interesting is glycine. As it has been shown recently that microcrystals based on glycine reveal both piezoelectric and ferroelectric properties[40,56,57] and thus present significant interest for biomedical and electronic applications. Glycine (the simplest amino acid from all existing) is one of basic and important elements in biology as it serves as a building block for many biological macromolecules, such as peptides or proteins.[43] The main structural and physical properties of glycine-based systems are reviewed in this section, mainly in the context of their notable piezoelectric and ferroelectric properties.

A. Main peculiarities of glycine and glycine-based crystal systems

Depending on the solution type and crystallization conditions, crystalline glycine can exist in three polymorphic with different physical properties: α, β, and γ. The structural peculiarities and physical properties of these polymorphic forms have been investigated in the past.[58–60] However, there are only few attempts to evaluate piezoelectric properties of these materials.[40,56] $\alpha-$glycine has a centrosymmetric structure (space group P21/n) and consequently cannot have piezoelectric property (the individual molecular dipole of glycine molecule is compensated with that in opposite direction), while the γ- and β-glycine possess non-centrosymmetric structure (with two differently formed and oriented by individual dipoles of each glycine molecules). Therefore, they were studied in a more detail in a series of papers.[40,56,57,61–67]

One of the specific features of all glycine crystals phases is related to its hydrogen-bonded network system. According to the modeling results of β-glycine,[62] there are two main type of H-bonds: within layer: H-bond with length $L \approx 1.179$ Å and inter-layer: H-bond with length $L \sim 2.75$ Å. As derived from IR-experiments,[58] hydrogen bonds within the layer are stronger than the inter-layer ones in γ- and β-glycine. The network of hydrogen bonds plays an essential role in organization of the crystal structure of glycine. In β-glycine, each single layer is held to each another by weaker hydrogen bonds than those contributing to the formation of double layers in the α-form; the weakest hydrogen bond in the a-form being weaker than the weakest hydrogen bond in the γ-form. The correlation between the N…H stretching frequency and the thermodynamic energy Δsol$H$m was examined in three phases of glycine.[64] This result confirms again the importance of the network of the hydrogen bonds for the crystal structure. Based on analysis of Δsol$H$m, the phases can be arranged in a descending order of their absolute values of the lattice energies: $\gamma- > \alpha- > \beta$-modification.[64]

B. Polarization, piezoelectric, and ferroelectric properties of glycine-based structures

The most interesting structures for applications are β-glycine (space group $P2_1$) and γ-glycine (space group $P3_2$)[63–67] because of their useful functional properties. Molecular modeling results using unrestricted Hartry-Fock (UHF) quantum-chemical semi-empirical PM3 method[62] predict polarizability value $\alpha \sim 29$ a.u. ~ 4.5 Å^3 in a good

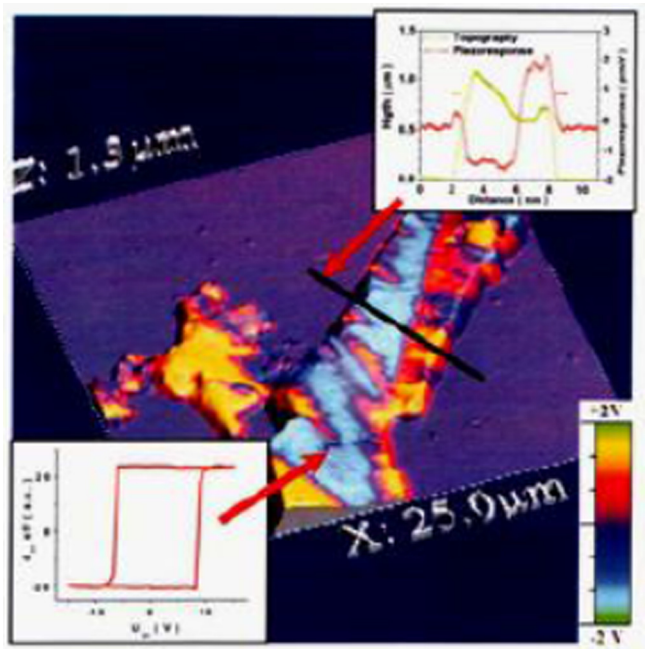

FIG. 10. PFM image obtained in glycine microcrystal. Insets are representative piezoresponse hysteresis loop and cross sections of image. Adapted from Ref. 40.

agreement with literature data.[68,69] It was shown that the individual glycine dipole provides polarization $P \sim 0.6\,C/m^2$ that can be switched under an applied external electric field $E_c \sim 1$ GV/m. These data give an evidence of the possible ferroelectric-like behaviour of glycine molecule and consequently leads to an incentive to studying such properties in glycine crystals. But, the realization of this opportunity depends on the possibility of the growth of specific polymorphic form in a crystal of sufficiently big dimensions.

Indeed, nanoscale ferroelectricity was observed in glycine microcrystals by the PFM method.[40] As-grown domains and polarization switching were confirmed by SS-PFM in this work. Figure 10 shows areas with different polarization directions (ferroelectric 180° domains with polarization vectors oriented normal to the substrate) that were spontaneously formed in glycine microcrystals. This was proven by the absence of the IP (lateral) response (see inset to Fig. 10), irrespective of the scanning direction. Relatively sharp boundaries separating antiparallel polarization domains were found with the wedge-like domain morphology typical for ferroelectrics. Piezoresponse hysteresis loop (Fig. 10) is a clear signature of polarization switching on the local scale. It provides several important parameters of the ferroelectric material, such as values of the piezoelectric coefficient (proportional to the polarization), nucleation bias (the threshold for the piezocontrast increase), imprint (the shift of the loop along the bias axis), and work of switching (directly proportional to the area encompassed by the loop).

Figure 11 shows molecular crystal structures in γ- and β-glycine for two projections of hydrogen bonds network and resulting dipole moment. The main difference for these structures is that for β-glycine we have strongly oriented hydrogen-bond network along OZ axis with total dipole moment and polarization oriented in this direction. The calculated value of polarization by UHF PM3 method for modelled molecular cluster from 27 individual glycine molecules is $P \approx Pz = 0.17\,C/m^2$ for this γ-glycine polymorphic crystal structure. The calculated volume of γ-glycine lattice unit cell is $V_c = 219.8\ A^3$. In β-glycine, the structure is different (molecular model consists of 16 molecules) with hydrogen bonds in XOZ plane and between layers. In this case, the dipole moment has several components, which are oriented under various

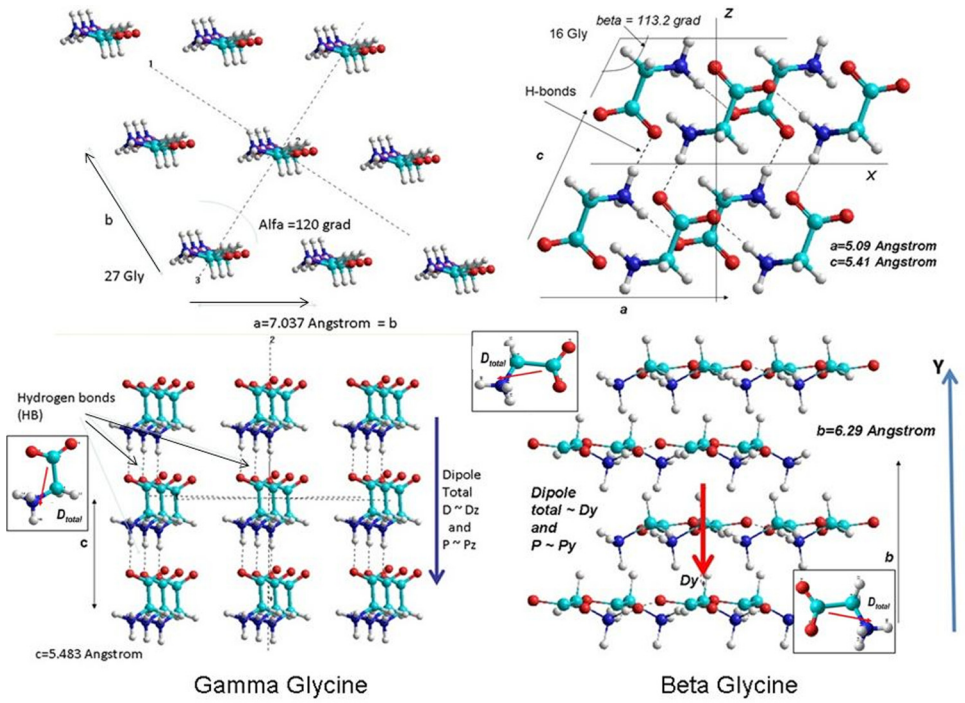

FIG. 11. Molecular models of two polymorphic glycine (β and γ) crystal structures. Insets show schematics of the individual dipole moment orientations of glycine molecules for β and γ polymorphs.

angles to main axis with oppositely directed and compensated components in the XOZ plane. Along the OY axis, the components sum up and total resulting polarization is directed along this axis. The calculated polarization components are smaller than in the previous case, $P \approx Py \approx 0.1.0.13\ C/m^2$. Such structural features lead to an easier rotation of β-glycine under an applied electric field as compared to γ-glycine where each individual molecule is fixed in a more stable position. The calculated volume of the β-glycine lattice unit cell is $V_c = 158.9\ A^3$ which is smaller as compared to γ-glycine. Estimation of coercive electric field gives $E_c \approx 30.50$ MV/cm along OZ axis, and it is hard (almost impossible) to switch polarization in this case. For β-glycine, the coercive field Ec ≈ 10…15 MV/cm is much smaller and switching is possible. Indeed, this was observed in PFM experiments.[40,62]

IV. PIEZOELECTRICITY AND FERROELECTRICITY IN DI-PHENYLALANINE PEPTIDE NANOTUBES

Self-assembled diphenylalanine (FF) peptide nanotubes (PNTs) represent a novel class of bottom-up fabricated biomaterials. The discovery of strong piezoelectric activity, temperature-dependent spontaneous polarization, and phase transition[41,70–72] in these aromatic dipeptides established them as functional nanomaterials with a range of possible applications. The inorganic tubes made of Pb(Zr,Ti)O3 are potential candidates for microfluidics THz emission.[73] Organic ferroelectrics[1] offer a potential cost advantage, flexible deposition and control, as well as self-assembly features, all of which are not currently available in conventional perovskites. Peptide-based systems are of particular importance from the biological of view, as models for biological membranes, amyloid fibrils, etc.[74,75] For this group of materials, tube-like structures are easily formed by stacking aromatic rings through the formation of hydrogen bonds between functional groups in the backbone structure, related to aromatic π-π interactions.[76] A common self-assembly process for small aromatic di-peptides involves the assembly of FF, NH2-Phe-Phe-COOH, monomers into PNTs. The structure of di-phenylalanine was studied in detail by Gorbitz[77–79] and by the group of Gazit.[75,76,80–82] They are made from amino acids molecules, self-assembled as uniquely stable tubes with hydrophilic hollows, and possess high Young's modulus and chemical stability.[82]

It was shown[41] that FF PNTs are also strongly piezoelectric, with the orientation of polarization along the tube axis. They demonstrate a temperature-dependent polarization response as common to ferroelectrics.[70] The molecular

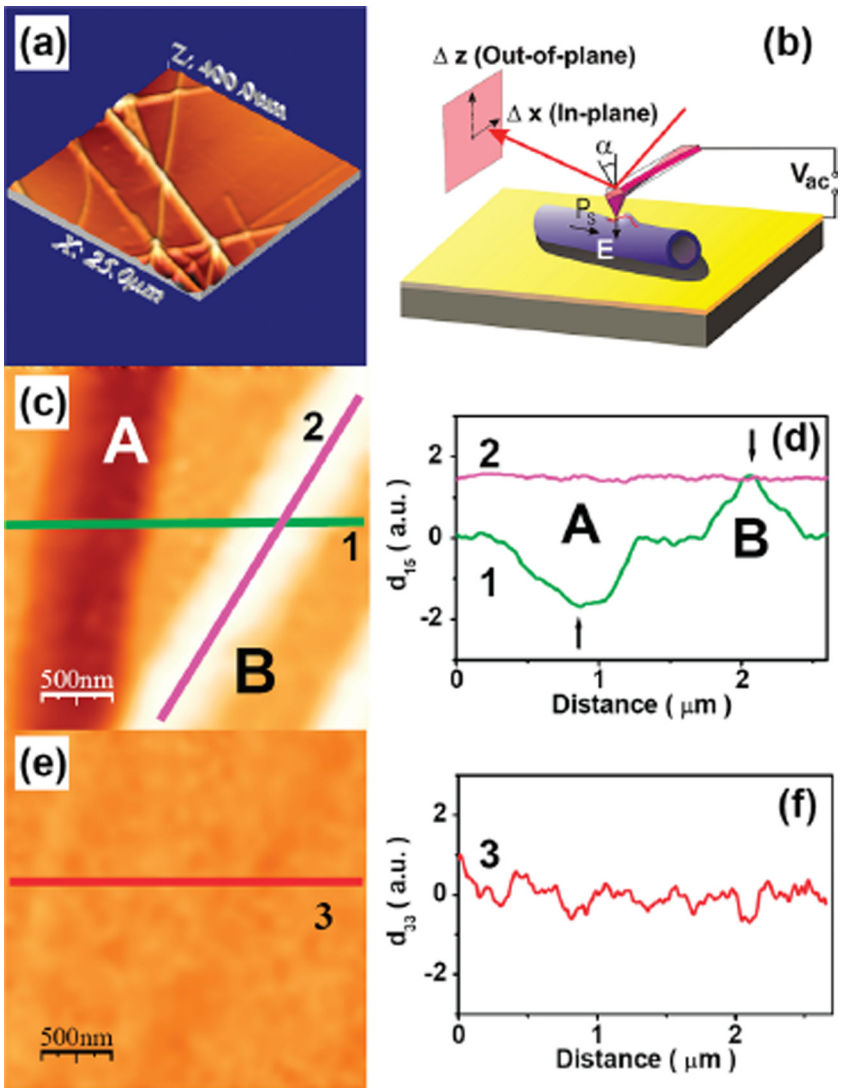

FIG. 12. Schematic of the AFM/PFM experiments: (a) Topography of as deposited PNTs on Au coated sub strate (scan 25 × 25 μm^2), (b) sche matic of the nanoscale in plane (IP) measurements by PFM, (c) IP piezor esponse of two tubes (A and B) with oppositely directed polarizations, (d) cross sections of the IP image across (1) and along (2) PNT tube axis, dem onstrating different signs and uniform ity of polarization, (e) OOP image of the same tubes, and (d) cross section of (e) along line 1. V_{ac} 2.5 V, f 5 kHz. Reprinted with permission from Kholkin *et al.*, ACS Nano **4**, 610 (2010). Copyright 2010 American Chemical Society.

modeling of the structure and physical properties, as well as the dynamic behavior under electrical field and temperature variation, was performed by molecular modeling and molecular dynamic (MD) simulation, using HypeChem versions 7.52 and 8.01.[83] A short overview of these results is given in the next sections.

A. PFM study of ferroelectric and piezoelectric properties of FF PNTs

Figure 12 shows the representative SEM and PFM images of the fabricated PNTs, assembled horizontally and vertically on metallized substrates. Strong piezoelectric contrast was seen on both horizontal (via lateral PFM signal, inset to Fig. 13(a)) and vertical tube assemblies (via vertical PFM, inset to Fig. 13(b)). The estimate of the effective longitudinal piezoelectric coefficient d_{33} measured on vertical tubes yields maximum values of about 30 pmV ^{1}, i.e., exceeding that for $LiNbO_3$.

Figure 14(b) represents the variation of the average shear PFM contrast with increasing temperature measured on horizontal tubes. The contrast gradually decreases with temperature, demonstrating monotonic d_{15} dependence and ultimate disappearance of piezoresponse at about 150 °C. It should be noted that the contrast becomes irreversible if the sample is heated above 100 °C, i.e., it is not recovered after cooling down to room temperature and remains practically zero after heating up to 140 150 °C. This hints at the possible phase transformation to another phase on heating, as no visible degradation of the topography was found.

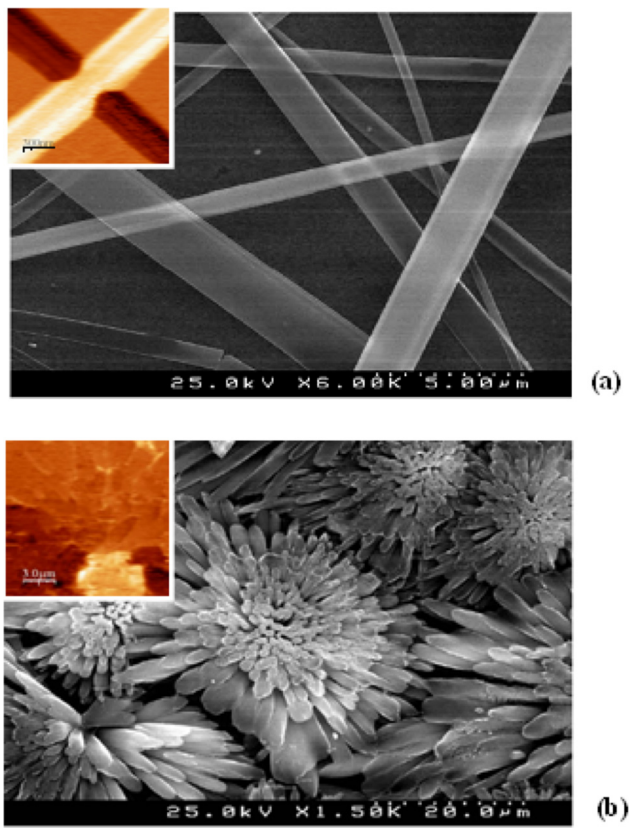

FIG. 13. Representative SEM images of horizontal (a) and vertical (b) pep tide nanotube array. Insets show corresponding PFM images. Reproduced by permission from Heredia *et al.*, J. Phys. D **43**, 462001 (2010). Copyright 2010 by IOP Publishing.

Figure 14(a) shows the temperature dependence of SHG intensity measured on vertical tubes (both heating and cooling runs), which are compared with the MD calculations[5] using HyperChem software.[83] The results are, in general, consistent with the temperature-dependent PFM contrast measurements. Eventually, the SHG signal decreases at ~130 °C (irreversibly as shown by the cooling curve). It should be noted that these data are consistent with recent studies of thermal stability of PNTs.[82] These measurements revealed that FF PNTs exhibit a phase transition between two piezoelectric phases, as confirmed by the existence of piezoresponse both below and above the transition in the temperature range 100 150 °C. In general, the apparent decrease in the piezoelectric contrast and SHG intensity (Fig. 14) with temperature is a clear signature of an irreversible phase transformation to a high-symmetry phase, as is often observed in molecular crystals.[44,84]

The XRD patterns of the vertical PNTs were measured before and after temperature annealing at 150 °C for 1 h. In virgin samples (grown at room temperature), all observed peaks correspond to the expected hexagonal structure already reported for FF PNTs ($a = 24.071$ Å, $c = 5.456$ Å, $\alpha = 120°$, space group $P61$).[70] The diffraction peaks for annealed PNTs are apparently different, belonging to another crystalline phase. All diffraction peaks after annealing could be explained based on the appearance of an orthorhombic structure with the unit cell parameters: $a = 5.210$ Å, $b = 24.147$ Å, $c = 41.072$ Å.[5,70]

These experimental results and observed structural transformation in FF PNTs were corroborated by molecular dynamic simulations, predicting an order disorder phase transition into a centrosymmetric (possibly, orthorhombic) phase with the antiparallel polarization orientation in neighbouring FF rings. Partial piezoresponse hysteresis in vertical nanotubes indicates incomplete polarization switching due to the high coercive field along the tube axis in virgin FF PNTs. All the attempts to switch polarization in this material were unsuccessful due to geometry and high coercive voltage observed in the nanoscale ferroelectric measurements.

B. Computational modeling of FF PNTs structures and properties

The molecular modeling of the structure and physical properties, as well as the dynamic behavior under electrical field and temperature variation, were performed by molecular modeling and MD simulation, using HypeChem versions 7.52 and 8.01.[5,6,70,72,83] The isolated ring with six dipeptides, as well the parallel stacking of two rings, were studied by the geometry optimization of the total energy, and MD runs using molecular mechanics (MM) methods (BIO CHARM) in combination with the first principle quantum approach (*ab initio* and PM3 semi-empirical, in UHF approximation).

The key point of the developed model is the self-consistent formation of the complex hydrogen bond network, which leads to the self-assembly of all molecular dipoles in

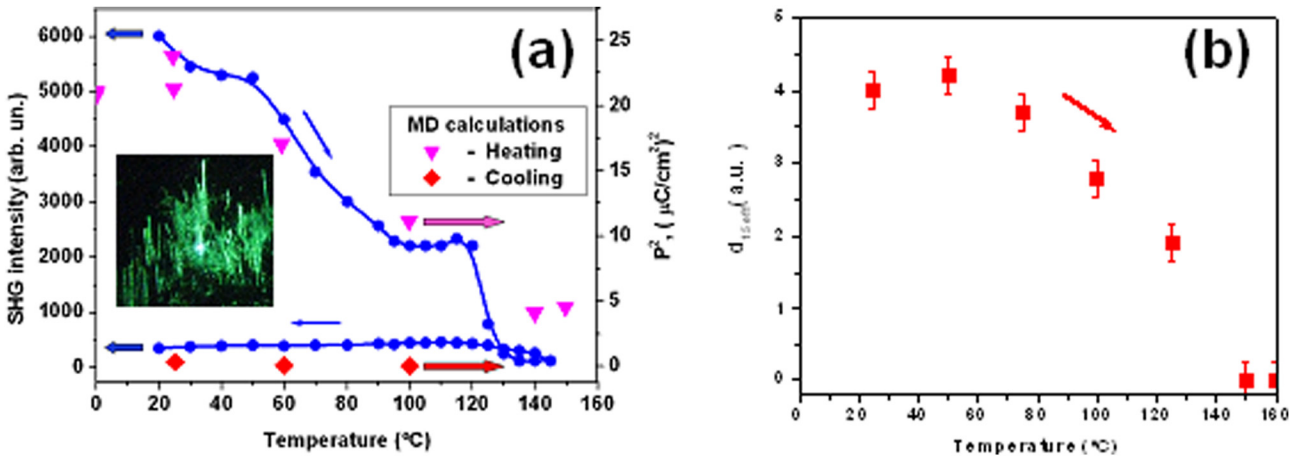

FIG. 14. Temperature dependencies of SHG (a) and PFM signals (b) for FF PNTs. The data points on SHG curves are compared with the MD calculations undertaken for parallel double stacked FF in the hexagonal phase (triangles) and anti parallel ones in the orthorhombic phase (diamonds). Reproduced by per mission from Heredia *et al*., J. Phys. D **43**, 462001 (2010). Copyright 2010 by IOP Publishing.

the system, with the emergence of a large total dipole and common co-orientation as a consequence. As a result, existence of the dielectric polarization at the molecular level is predicted. It was found that 6FF forms ordered rings (and further the hexagonal structure, *P*61) with inner and outer diameters of about 10.5 and 25 Å, respectively, connected by N H…O hydrogen bonds with O-H lengths of ≈1.65 Å and total N-O lengths of ≈2.7 Å. This is in a full agreement with the results by Gorbitz.[77] Furthermore, the calculations of the dipole moment predict the value of ≈1.3 Debye for a single 6FF ring, directed along the OZ hexagonal axis, corresponding to a spontaneous polarization of $P \approx 0.24\ \mu C/cm^2$.

The calculations of the dipoles and hydrogen bond interactions have resulted in the formation of FF PNTs having a polarization value given above. To reach the stable self-assembled formation, the HyperChem special option of geometry optimization was used. The searching for the energy minimum of the total potential energy surface (PES) of the molecular system by conjugated gradient approach at each PES point (with complex calculation of total system energy by the quantum-chemical semi-empirical method PM3) was applied.

The optimization (by PM3 method) for this model leads to a huge increase of dipole moment from ≈1.3 Debye up to Dt ≈ 42 Debye (polarization $P \approx 4.0\ \mu C/cm^2$), and furthermore up to a value of Dt ≈ 52 Debye and polarization value $Ps \approx 5\ \mu C/cm^2$.[5,6,70] These two 6FF rings are connected by N-H…O hydrogen bonds with O-H lengths of ≈1.88 Å and total N-O lengths of ≈2.9 Å. After self-consistent optimization of the system (using HyperChem with PM3 approximation), the cooperative alignment of self-assembled dipoles and hydrogen bonds results in the total increase of dipole moment of the system of more than 10 times. This is a direct evidence of ferroelectric ordering in this system. The resulting value of polarization just after optimization is approximately P ≈ 3.336 D/V ≈ 0.0401 C/m^2 ≈ 4 μC/cm^2, which is directed along the OZ axis of FF PNT (where D is the total dipole and V is the volume of whole system).

Further calculations were intended to understand why the polarization (and piezoelectric response) could not be switched in the direction along the main OZ axis. The calculations by PM3 (as well by BIO CHARM) methods were performed under applied electric field along this OZ axis for different values of the field.[5,70,72] The results clearly show that, owing to the huge dipole moment that exists inside FF PNT and oriented along OZ axis, the switching of the dipole moment (as well the total polarization) is hardly possible because of extremely high coercive field corresponding to the value of 30 45 MV/cm (Fig. 15(a)). This prediction is fully consistent with the experimental result (Fig. 15(b)),

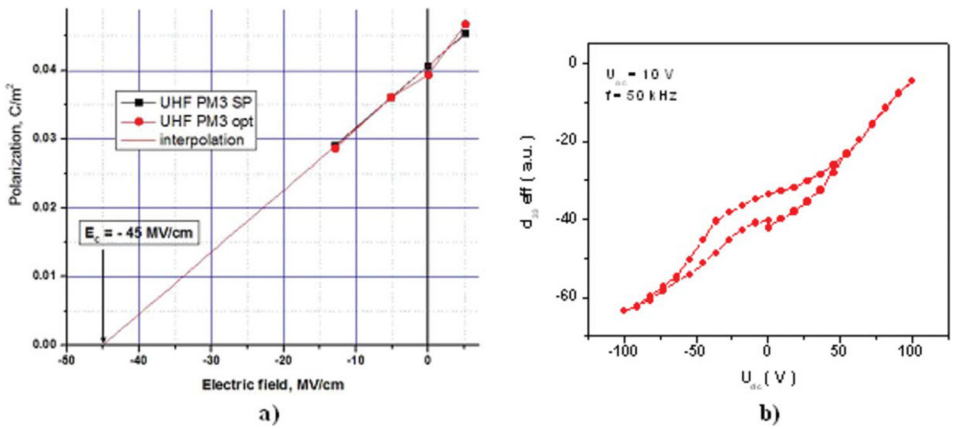

FIG. 15. Influence of applied electric field along OZ axis of FF PNTs: (a) on the polarization values, (b) on piezor esponse. (Color figure available online). Reproduced by permission from Heredia *et al*., J. Phys. D **43**, 462001 (2010). Copyright 2010 by IOP Publishing.

which shows partial hysteresis in the effective d_{33} vs. applied bias dependence. Since the available electric field from the PFM tip is sufficiently low (in the first approximation ≈100 200 kV/cm under a bias of 10 V), FF PNTs cannot be switched thus making this material inapplicable for high density data storage. Unfortunately, higher bias destroys the tubes. Molecular simulations made under an electrical field are in line with the experimental observation and showed that an antiparallel field of about 5 MV/cm is only able to decrease the polarization value by about 12%.[5,6]

C. Phase transition in FF PNTs

However, another opportunity may still exist for the radial switching (perpendicular to PNT axis direction) as it will be shown below. This is because FF PNTs are prone to the irreversible structural transformation in the temperature range ≈140 150 °C. MD runs and molecular simulations at different temperatures were performed to understand the properties of FF PNTs after this transformation. The calculated total polarization of FF PNTs decreases with increasing temperature and in the temperature region above ≈100 °C the molecular structure becomes very deformed and disordered, being a signature of structural transformation. The result is fully consistent with experimentally obtained SHG and PFM data, i.e., the average dipole moment gradually decreases as a function of temperature. The polarization is about 5 μC/cm^2 at 25 °C and decreases down to the value ≈2 μC/cm^2 at 100 °C. Note that in Figure 14(a), the values plotted on the right axis are P^2, and that the transition is irreversible, with no recovery on cooling.

The observed phase transition between hexagonal and orthorhombic phases upon heating shows how the initial hexagonal unit cell could be transformed into an orthorhombic one via small deformation of FF rings. The mainframe of FF PNT structure consists of FF rings, formed from six individual FF molecules (6FF), in accordance with Gorbitz.[77] Each ring possesses a dipole moment P_s along the tubular OZ axis perpendicular to the ring plane, and forms the hexagonal structure out of four rings. Antiparallel (antiferroelectric phase) orientation of P_s for the neighboring 6FF rings results in novel orthorhombic structure with zero total polarization for annealed tubes.

The results for a parallel stacked FF ring model correspond to the hexagonal phase and the experimentally observed large dipole moment and high piezoelectric coefficient in unannealead structures,[5,6,70] while the anti-parallel orientation of neighboring tubes corresponds to the orthorhombic phase with a very small total dipole moment. It was suggested that the large polarization along OZ axis for the hexagonal phase is due to a cooperative dipole effect (as common to ferroelectric systems), while the orthorhombic phase is similar to antiferroelectrics, and polarization switching would be possible if a high-enough electric field is applied along this axis.[5,70,72] This model is in line with the experimental XRD data, and the observed orthorhombic structure upon annealing.[70] Upon cooling, this phase persists down to a room temperature, being metastable for an extended period of time.

D. Diphenylalanine peptide nanotubes: Evidence of ferroelectricity

The observed phase transformation from the hexagonal polar to the orthorhombic antipolar state is consistent with the temperature dependence of the dielectric permittivity studied on pressed pellets of FF PNTs. The observed Curie-Weiss behavior of dielectric permittivity is in a full agreement with the proposed model of ferroelectric phase transition (Fig. 16).[72] The fitted value of the Curie-Weiss point is $T_c \approx 142.5$ °C with Curie-Weiss constant $C_{wb} = 230$ K and extrapolation shows that T_{cwb} is about165 °C.[71,72] Assuming that the phase transition in FF PNT is close to the first order, we can estimate the Curie-Weiss constant below the phase transition temperature, C_{wa}, as $\approx 8C_{wb} \approx 1840$ K.[7] Moreover, this model allows us to explain the irreversible nature of the transition as revealed by SHG signal (Fig. 14(a), cooling branch): in this case, without an applied electric field, we have vanishing value of the total dipole moment due to full compensation of individual moments. It should be stated here that, according to Ryu and Park,[85] some additional structural transformation could occur under the prolonged annealing above 150 °C. This could lead to the conformational change from linear FF to cyclic FF with a 5.8% loss of mass due water evaporation (one molecule of water per FF molecule). This transformation occurs at higher temperatures and presumably under high pressure conditions.

The developed model allowed calculating several physical parameters of FF PNTs (polarizability α, electrostriction coefficient Q, coercive electric field E_c, dielectric permeability ε, piezoelectric coefficient d). These are presented in Table I for two different orientations of electric field. These parameters are useful for the interpretation of local piezoelectric measurements and could serve as input parameters for Finite Element Modeling (FEM) of the peptide nanostructures.

In conclusion, our molecular modelling and measurements revealed an important feature of the polarization behavior in self-assembled di-phenylalanine peptide

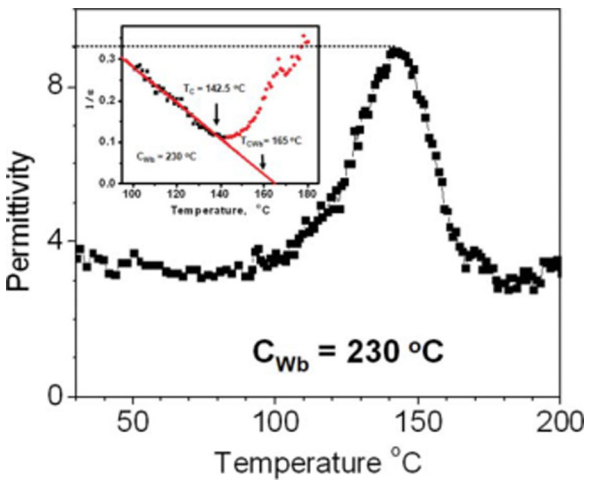

FIG. 16. Temperature dependence behavior of dielectric permittivity of annealed FF PNTs. Reprinted with permission from Bdikin *et al.*, Appl. Phys. Lett. **100**, 043702 (2012). Copyright 2012 Lincoln Taylor & Francis Copyright Clearance Center.

TABLE I. Physical parameters of FF PNTs obtained by molecular modeling.

Type of orientation	ΔD, Debye	ΔP, μC/cm^2	Q	S/(ΔP)^2, m^4/C^2	α	ΔD/ΔE, Å^3	E$_c$, MV/cm	ε	d	2εε$_0$QΔP, pm/V
Along OZ	∼2.0	∼0.2		∼350.0		∼280.0	30.0 45.0	∼4		∼50.0
Lateral OX	∼6.8	∼0.7		∼30.0		∼400.0	∼5.00	∼4		∼15.0

nanotubes. As was shown by MD runs and confirmed by PFM and SHG measurements, polarization gradually decreases from room temperature to ≈140 °C, and experiences an irreversible phase transformation from polar hexagonal to an orthorhombic crystalline phase with zero net polarization. This phase persists upon cooling to room temperature. Partial polarization switching is observed by the application of a strong electric bias to the PFM tip along the FF PNT tubes main OZ axis, but in this case full switching is impossible due to the high coercive field (Fig. 15). These results are in line with ferroelectric-like ordering of hydrogen bonds between FF monomers, which break upon the temperature increase. This transformation is extremely important in view of the foreseeable applications of PNTs as sensors and actuators. However, if annealed and transformed to the orthorhombic structure, FF PNT can be switched in the radial direction, perpendicular to initial OZ axis of hexagonal structure.

V. CONCLUSIONS

In this work, we show that the smallest amino acid glycine and self-assembled diphenylalanine nanotubes possess notable piezoelectric and ferroelectric properties that are consistent with the general notion of the ubiquitous presence of ferroelectric ordering in many biological macromolecular structures including lipids, ion channels, proteins, etc. This further underlines the significance of biopiezoelectric and bioferroelectric phenomena in living organisms. Once we understand the role of ferroelectricity and piezoelectricity in complex hierarchical biosystems, it will be easier to design novel devices which mimic nature, or are inspired by it. The results reported here are the first nanoscale experiments on amino acids and peptides and they are explained by the idealized molecular models. However, they reproduce the essential features of the phase transformations. For example, the observed high temperature phase in FF PNTs with oppositely oriented and mutually compensated dipoles could be considered as an antiferroelectric phase, similar to some examples of biologically ordered molecular structures, e.g., in lipids. Obviously, further experiments and simulations are necessary for the full understanding of the role of bioferroelectricity and biopiezoelectricity in the human body. On the contrary, the development of bioorganic artificial materials with enhanced piezoelectric and ferroelectric properties is of high importance for future biologically compatible sensors, actuators, transducers, and other electronic components.

ACKNOWLEDGMENTS

The work was supported by the European Commission within FP7Marie Curie Initial Training Network "Nanomotion" (Grant Agreement No. 290158) and by the FP7 project "PodiTrodi."

[1]S. Horiuchi and Y. Tokura, Nature Mater. **7**, 357 (2008); Adv. Mater. **23**, 2098 (2011).
[2]F. Kagawa, S. Horiuchi, N. Minami, S. Ishibashi, K. Kobayashi, R. Kumai, Y. Murakami, and Y. Tokura, Nano Lett. **14**, 239 (2014).
[3]B. Coste, B. Xiao, J. S. Santos, R. Syeda, J. Grandl, K. S. Spencer, S. E. Kim, M. Schmidt, J. Mathur, A. E. Dubin, M. Montal, and A. Patapoutian, Nature **483**(7388), 176 (2012).
[4]S. E. Kim, B. Coste, A. Chadha, B. Cook, and A. Patapoutian, Nature **483**(7388), 209 (2012).
[5]V. S. Bystrov, E. Paramonova, I. Bdikin, S. Kopyl, A. Heredia, R. Pullar, and A. Kholkin, Ferroelectrics **440**, 3 (2012).
[6]V. S. Bystrov, I. Bdikin, A. Heredia, R. C. Pullar, E. Mishina, A. S. Sigov, and A. L. Kholkin, in *Piezoelectric Nanomaterials for Biomedical Applications*, edited by G. Ciofani and A. Menciassi (Springer Verlag, Berlin Heidelberg, 2012), pp. 187 211.
[7]M. E. Lines and A. M. Glass, *Principles and Applications of Ferroelectrics and Related Materials* (Clarendon Press, Oxford, 1977).
[8]J. F. Nye, *Physical Properties of Crystals: Their Representation by Tensors and Matrices* (Oxford University Press, NY, 1957).
[9]E. Fukada, Nature **166**, 772 (1950).
[10]E. Fukada, J. Phys. Soc. Jpn. **10**, 149 (1955).
[11]E. Fukada and I. Yasuda, J. Phys. Soc. Jpn. **12**, 1158 (1957).
[12]E. Fukada and I. Yasuda, Jpn. J. Appl. Phys., Part 1 **3**, 117 (1964).
[13]H. R. Leuchtag, *Voltage Sensitive Ion Channels: Biophysics of Molecular Excitability* (Springer, Dordrecht, 2008).
[14]H. R. Leuchtag and V. S. Bystrov, Ferroelectrics **220**, 157 (1999).
[15]N. Amdursky, P. Beker, J. Schklovsky, E. Gazit, and G. Rosenman, Ferroelectrics **399**, 107 (2010).
[16]S. B. Lang, Ferroelectrics **34**, 3 (1981).
[17]E. Fukada, Q. Rev. Biophys. **16**, 59 (1983).
[18]S. B. Lang, A. A. Marino, G. Berkovic, M. Fowler, and K. D. Abreo, Bioelectrochem. Bioenerg. **41**, 191 (1996).
[19]S. B. Lang, Nature **212**, 704 705 (1966); **224**, 798 (1969).
[20]S. B. Lang, IEEE Trans. Dielectr. Electr. Insul. **7**, 466 (2000).
[21]A. Gruverman, B. J. Rodriguez, and S. V. Kalinin, in *Scanning Probe Microscopy: Electrical and Electromechanical Phenomena at the Nanoscale* (Springer, New York, 2007), Vol. 2, pp. 615 633.
[22]T. Li and K. Zeng, J. Appl. Phys. **113**, 187202 (2013).
[23]M. Pal, R. Guo, and A. Bhalla, Mater. Res. Innovations **17**, 442 (2013).
[24]H. Athenstaedt, Ann. N. Y. Acad. Sci. **238**, 68 (1974).
[25]Y. Liu, Y. Zhang, M. J. Chow, Q. N. Chen, and J. Li, Phys. Rev. Lett. **108**, 078103 (2012).
[26]Y. Liu, Y. Wang, M. J. Chow, N. Q. Chen, F. Ma, Y. Zhang, and J. Li, Phys. Rev. Lett. **110**, 168101 (2013).
[27]H. Frolich, Riv. Nuovo Cimento **7**, 399 (1977); A. Muller, Phys. Lett. A **96**, 319 (1983).
[28]I. Tasaki, "Evidence for phase transition in nerve fibres, cells and synapses," Ferroelectrics **220**, 305 316 (1999).
[29]L. A. Beresnev, S. A. Pikin, and W. Haase, Condens. Matter News **1**(8), 13 (1992).
[30]Y. Palti and W. J. Adelman, Jr., J. Membr. Biol. **1**, 431 (1969).
[31]I. Ermolina, A. Strinkovski, A. Lewis, and Yu. Feldman, J. Phys. Chem. B **105**, 2673 (2001).
[32]V. S. Bystrov and N. K. Bystrova, "Bioferroelectricity and optical properties of biological systems," in Proceedings of SPIE, Vol. 5122. Advanced Organic and Inorganic Optical Materials, edited by Andris Krumins, Donats Millers, Inta Muzikante, Andris Sternberg, and Vismant Zauls, (SPIE, Bellingham, WA, 2003), pp. 132 136.
[33]J. A. Brown and J. A. Tuszynski, Ferroelectrics **220**, 141 (1999).
[34]J. A. Tuszynski, T. J. A. Craddock, and E. J. Carpenter, J. Comput. Theor. Nanosci. **5**, 2022 (2008).

[35]A. L. Kholkin, S. V. Kalinin, A. Roelofs, and A. Gruverman, in *Scanning Probe Microscopy: Electrical and Electromechanical Phenomena at the Nanoscale* (Springer, NY, 2007), Vol. 1, pp. 173 214.
[36]N. Balke, I. Bdikin, S. V. Kalinin, and A. L. Kholkin, J. Am. Ceram. Soc. **92**, 1629 (2009).
[37]S. V. Kalinin, B. J. Rodriguez, J. Shin, S. Jesse, V. Grichko, T. Thundat, A. P. Baddorf, and A. Gruverman, Ultramicroscopy **106**, 334 (2006).
[38]S. V. Kalinin, S. Jesse, B. J. Rodriguez, K. Seal, A. P. Baddorf, T. Zhao, Y. H. Chu, R. Ramesh, E. A. Eliseev, A. N. Morozovska, B. Mirman, and E. Karapetian, Jpn. J. Appl. Phys., Part 1 **46**, 5674 (2007).
[39]B. Chen and H. Gao, Physics **5**, 19 (2012).
[40]A. Heredia, V. Meunier, I. K. Bdikin, J. Gracio, N. Balke, S. Jesse, A. Tselev, P. Agarwal, B. G. Sumpter, S. V. Kalinin, and A. L. Kholkin, Adv. Funct. Mater**.** **22**, 2996 (2012).
[41]A. Kholkin, N. Amdursky, I. Bdikin, E. Gazit, and G. Rosenman, ACS Nano **4**, 610 (2010).
[42]A. Heredia, I. K. Bdikin, M. Machado, S. Yudin, V. M. Fridkin, I. Delgadillo, and A. L. Kholkin, J. Phys. D **43**, 335301 (2010).
[43]L. Lehninger, *Biochemistry: The Molecular Basis of Cell Structure and Function* (Publishers, Inc., New York, 1972).
[44]*Ferroelectric Liquid Crystals: Principles, Properties and Applications*, edited by J. W. Goodby, R. Blinc, N. A. Clark, S. T. Lagerwall, M. A. Osipov, S. A. Pikin, T. Sakurai, K. Yoshino, and B. Zeks (Gordon and Breach, Philadelphia, 1991).
[45]G. W. Gray, *Molecular Structures and the Properties of Liquid Crystals* (Academic Press, London, 1962).
[46]G. Brown and J. J. Wolken, *Liquid Crystal and Biological Structures* (Academic Press, New York, 1979).
[47]S. Abeygunaratne, A. J. Jakli, G. Milkereit, H. Sawade, and V. Vill, Phys. Rev. E **69**, 021703 (2004).
[48]W. Curatolo, Biochim. Biophys. Acta **906**, 111 (1987).
[49]T. Niori, T. Sekine, J. Watanabe, T. Furukawa, and H. Takezoe, J. Mater. Chem. **6**, 1231 (1996).
[50]D. R. Link, G. Natale, R. Shao, J. E. Maclennan, N. A. Clark, E. Korblova, and D. M. Walba, Science **278**, 1924 (1997).
[51]W. Weissflog, C. Lischka, S. Diele, G. Pelzl, and I. Wirth, Mol. Cryst. Liq. Cryst. **328**, 101 (1999).
[52]V. S. Bystrov, I. K. Bdikin, D. A. Kiselev, S. Yudin, V. M. Fridkin, and A. L. Kholkin, J. Phys. D: Appl. Phys. **40**, 4571 (2007).
[53]V. S. Bystrov, N. K. Bystrova, E. V. Paramonova, G. Vizdrik, A. V. Sapronova, M. Kuehn, H. Kliem, and A. L. Kholkin, J. Phys.: Condens. Matter. **19**, 456210 (2007).
[54]D. Conklin, T. H. Park, S. Nanayakkara, M. Therien, and D. A. Bonnell, Adv. Funct. Mater. **21**, 4712 (2011).
[55]V. V. Lemanov, S. N. Popov, and G. A. Pankova, Physics of Solid State **44**, 1929 (2002); Ferroelectrics **285**, 207 (2003).
[56]D. Isakov, E. M. Gomes, I. Bdikin, B. Almeida, M. Belsley, M. Costa, V. Rodrigues, and A. Heredia, Cryst. Growth Des. **11**, 4288 (2011).
[57]E. Seyedhosseini, M. Ivanov, V. Bystrov, I. Bdikin, P. Zelenovskiy, V. Ya. Shur, A. Kudryavtsev, E. D. Mishina, A. S. Sigov, and A. L. Kholkin, Cryst. Growth Des. **14**, 2831 (2014).
[58]E. V. Boldyreva, V. A. Drebushchak, T. N. Drebushchak, I. E. Paukov, Y. A. Kovalevskava, and E. S. Shutova, J. Therm. Anal. Calorim. **73**, 409 418 (2003).
[59]R. E. Marsh, Acta Crystallogr. **11**, 654 (1958).
[60]G. L. Perlovich, L. K. Hansen, and A. Bauer Brandl, J. Therm. Anal. Calorim. **66**, 699 (2001).
[61]D. Isakov, D. Petukhova, S. Vasilev, A. Nuraeva, T. Khazamov, E. Seyedhosseini, P. Zelenovskiy, V. Shur, and A. Kholkin, "In Situ Observation of the Humidity Controlled Polymorphic Phase Transformation in Glycine Microcrystals," Cryst. Growth Des. (published online).
[62]E. Seyedhosseini *et al*., "Domain structure and polarization switching in beta glycine microcrystals" (unpublished).
[63]V. S. Bystrov, E. Seyedhosseini, I. Bdikin, S. Kopyl, S. M. Neumayer, J. Coutinho, and A. L. Kholkin, "BioFerroelectricity: Glycine and Thymine nanostructures computational modeling and ferroelectric properties at the nanoscale," Ferroelectrics (in press).
[64]E. V. Boldyreva, V. A. Drebushchak, T. N. Drebushchak, I. E. Paukov, Y. A. Kovalevskava, and E. S. Shutova, J. Therm. Anal. Calorim. **73**, 419 428 (2003).
[65]Y. Iitaka, Acta Crystallogr. **14**, 1 (1961).
[66]Y. Iitaka, Acta Crystallogr. **13**, 35 (1960).
[67]Z. Latajka and H. Ratalczak, J. Phys. Chem. **83**, 2785 (1979).
[68]K. Yamada, A. Saiki, H. Sakaue, S. Shingubara, and T. Takahagi, Jpn. J. Appl. Phys., Part 1 **40**, 4829 (2001).
[69]K. R. Wilson, D. S. Peterka, M. Jimenez Cruz, S. R. Leone, and M. Ahmed, Phys. Chem. Chem. Phys. **8**, 1884 (2006).
[70]A. Heredia, I. Bdikin, S. Kopyl, E. Mishina, S. Semin, A. Sigov, K. German, V. Bystrov, and A. L. Kholkin, J. Phys. D **43**, 462001 (2010).
[71]I. Bdikin, V. Bystrov, I. Delgadillo, J. Gracio, S. Kopyl, E. Mishina, A. Sigov, and A. L. Kholkin, J. Appl. Phys. **111**, 074104 (2012).
[72]I. K. Bdikin, V. Bystrov, S. Kopyl, R. Lopes, I. Delgadillo, J. Gracio, E. Mishina, A. Sigov, and A. L. Kholkin, Appl. Phys. Lett. **100**, 043702 (2012).
[73]J. F. Scott, H. J. Fan, S. Kawasaki, J. Banys, M. Ivanov, J. Macutkevic, R. Blinc, V. V. Laguta, P. Cevc, J. S. Liu, and A. L. Kholkin, Nano Lett. **8**, 4404 (2008).
[74]J. D. Hartgerink, J. R. Granja, R. A. Milligan, and M. R. Chadiri, J. Am. Chem. Soc. **118**, 43 (1996).
[75]M. Reches and E. Gazit, Nat. Nanotechnol. **1**, 195 (2006).
[76]E. Gazit, FASEB J. **16**, 77 (2002).
[77]C. H. Gorbitz, Chem. Eur. J. **7**, 5153 (2001).
[78]C. H. Gorbitz, New J. Chem. **27**, 1789 (2003).
[79]C. H. Gorbitz, Chem. Commun. **2006**, 2332 2334 (2006).
[80]V. L. Sedman, L. Adler Abramovich, S. Allen, E. Gazit, and S. J. B. Tendler, J. Am. Chem. Soc. **128**, 6903 (2006).
[81]N. Kol, L. Adler Abramovich, D. Barlam, R. Z. Shneck, E. Gazit, and I. Rousso, Nano Lett. **5**, 1343 (2005).
[82]L. Adler Abramovich, M. Reches, V. L. Sedman, S. Allen, S. J. B. Tendler, and E. Gazit, Langmuir **22**, 1313 (2006).
[83]*HyperChem 7.5, Tools for Molecular Modeling; HyperChem 8.0, Professional Edition* (Hypercube. Inc., Gainesville, 2002 2010).
[84]J. Bernstein, *Polymorphism in Molecular Crystals* (Clarendon, Oxford, 2002).
[85]J. Ryu and C. B. Park, Biotechnol. Bioeng. **105**, 221 (2010).